Organic Electronics 15 (2014) 3144–3153

Contents lists available at ScienceDirect

Organic Electronics

journal homepage: www.elsevier.com/locate/orgel

Theoretical insight into the deep-blue amplified spontaneous emission of new organic semiconductor molecules

Lin Ma, Zhaoxin Wu *, Ting Lei, Yue Yu, Fang Yuan, Shuya Ning, Bo Jiao, Xun Hou

Key Laboratory of Photonics Technology for Information, School of Electronic and Information Engineering, Xi'an Jiaotong University, Xi'an 710049, PR China

ARTICLE INFO

Article history:
Received 29 May 2014
Received in revised form 7 August 2014
Accepted 12 August 2014
Available online 18 September 2014

Keywords:
Density functional theory
Amplified spontaneous emission
Franck–Condon factor
Huang–Rhys factor
Vibrational modes
Four-level energy level scheme

ABSTRACT

As for the lasing of organic semiconductor materials, novel semi-conducting materials N,N′-bis(3-methylphenyl)-N,N′-diphenyl-[1,1′:4′,1″-terphenyl]-4,4″-diamine (BMT-TPD) and N,N′-bis(3-methylphenyl)-N,N′-diphenyl-[1,1′:4′,1″:4″,1‴-quaterphenyl]-4,4‴-diamine (BMQ-TPD) were synthesized. In contrast to the N,N′-diphenyl-N,N′-bis(3-methylphenyl)-(1,1′-biphenyl)-4,4′-diamine (TPD), the well known organic gain medium for the lasing, the two new materials have lower amplified spontaneous emission (ASE) thresholds and enhanced lasing performance. The molecular geometries in the electronic ground state and the first optically excited state as well as the vibrational modes of the three compounds have been studied by means of the dependent density functional theory (DFT). Theoretical analysis shows that, accompanying with the increased number of central phenyl rings, the uniform high-frequency modes (around at 1200, 1300 and 1650 cm^{-1}) of the three compounds are enhanced, which is driven by the C—H bending and C—C stretching in the central phenyl rings. Correspondingly, the enhanced vibration strength of the high-frequency modes and reinforced vibronic peak intensity bring out the distinct "four-level" energy level scheme which benefits population inversion for lasing and leads to the decreased ASE threshold. These results indicate that the synthesized materials are good candidates to act as active laser materials and our work provides an insight into the lasing of small organic molecules.

1. Introduction

Molecular semiconducting materials, i.e. small molecules and oligomers, are one of the laser material classes investigated in recent years. Many of these systems have shown amplified spontaneous emission (ASE) thresholds much lower than those of traditional dyes, mostly due to the possibility of increasing the amount of materials in the films without significant PL quenching. N,N′-diphenyl-N,N′-bis(3-methylphenyl)-(1,1′-biphenyl)-4,4′-diamine (TPD) receives significant attention serve as solid state laser material over the years due to the broad photoluminescence and the tunable wide laser wavelength range [1–4] on account of its optical properties, absorption and emission behavior [5,6]. TPD shows stimulated emission in neat films that were fabricated by spin-coating, vacuum thermal evaporation and ink-jet printing as well as the blends that is diluted in polystyrene (PS) [7–10].

A lot of experiments have been carried out to study the ASE characteristics in TPD. It was considered that the factors of stokes shift, the radiative decay rate, the fluorescence lifetime and the fluorescence quantum yield are correlated with the stimulated emission phenomenon [10–12]. There are some density functional theoretical studies about the geometric structure and energetic of TPD [13,14], but as for the lasing mechanism of small molecules, up to now, few theoretical explanations were proposed in the molecu-

* Corresponding author. Tel./fax: +86 29 82664867.
E-mail address: zhaoxinwu@mail.xjtu.edu.cn (Z. Wu).

http://dx.doi.org/10.1016/j.orgel.2014.08.024
1566-1199/

lar structure and energy level point of view. Hence, the mechanism of organic semiconductor material for stimulated emission is ambiguity. In our previous work [15], we proposed that a handful of low-frequency modes and the strongly elongated high-frequency modes in the carbon rings contribute to distinct first vibronic sideband in the PL spectra. These formed an effective "four-level" system, which would be the key for lasing.

In this paper, based on TPD, following the idea in our previous work, we developed two compounds: N,N′-bis(3-methylphenyl)-N,N′-diphenyl- [1,1′:4′,1″-terphenyl] -4,4″-diamine (BMT-TPD) and N,N′-bis(3-methylphenyl)-N,N′-diphenyl- [1,1′:4′,1″:4″,1‴-quaterphenyl]-4,4‴-diamine (BMQ-TPD). On the one hand, in theory, by contrast with TPD, the increased number of central phenyl rings in BMT-TPD and BMQ-TPD lead to enhanced uniform strongly elongated high-frequency vibrational modes (around at 1200, 1300 and 1650 cm^{-1}). The high-frequency modes arise from the elongation of C—H in plane bending, C—C inter-ring stretching and C—C intra-ring stretching modes within the central phenyl rings. The intensive high-frequency vibrational modes, resulting in more remarkable vibronic peak in PL spectra, which is conductive to achieve more distinct "four-level" energy level scheme for the population inversion. Therefore, a significant low threshold is achieved. On the other hand, as we expected, the experimental results of resonant Raman peaks of BMT-TPD and BMQ-TPD were enhanced, which corresponds to reinforced elongation of high-frequency modes. Furthermore, the lower ASE thresholds for BMT-TPD and BMQ-TPD with deep-blue emission were achieved with the increased number of central phenyl rings, reduced by 2 times and 3.6 times compared with TPD respectively.

2. Experimental and theoretical methodology

2.1. Spectra measurement and ASE characteristics

Thin films, consisting of polystyrene (PS: inert polymer), doped with a certain amount (33 wt%, Sample:PS = 1:2) of TPD, BMT-TPD and BMQ-TPD (see Fig. 1), were spin-coated (around 500 nm) onto glass substrates at a speed of 3000 rpm and then the spin-coated films were annealed at 110 °C for 10 min in an oven.

Absorption and PL spectra were obtained by UV–Vis spectrophotometer (HITACHI U-3010, Japan) and Fluorescence Spectrometer (fluoromax-4 spectrofluorometer) respectively. As shown in Fig. 2, the normalized absorption spectra of TPD, BMT-TPD and BMQ-TPD possess two visible peaks and the lower energy peaks are the dominant. The PL

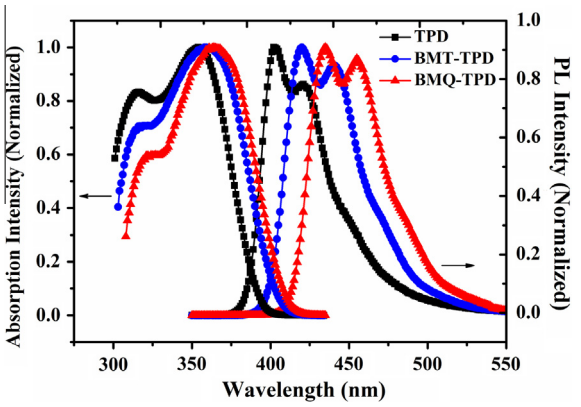

Fig. 2. Absorption and PL spectra of the three samples.

spectra of all three compounds show resolved vibrational progression, consisting of three emission peaks: a main band (0–0 transition) with a maximum at around 402 nm, 420 nm and 438 nm, the first visible vibronic peak (0–1 transition) at around 421 nm, 440 nm and 458 nm separately, and the second blurry vibronic peak (0–2 transition). Enhanced vibronic sideband, which was calculated as the product of the most strongly elongated in-plane modes, signify the intensive elongation of high-frequency modes with the increased number of central phenyl rings. The distinct first vibronic peak is beneficial to form distinct vibrational energy level included within electronic energy level.

To investigate ASE characteristics, the thin films were photopumped at normal incidence with a pulsed Nd:YAG laser (5.55 ns, 10 Hz) (Surelite I, Continuum Corp, USA), using the third harmonic (355 nm). The output beam of the Nd:YAG laser were shaped into a narrow stripe of approximately 1 mm width and 7 mm length by a cylindrical lens and an adjustable slit. The pump stripe was placed right up to the edge of the film where the emitted light was collected with a fiber spectrometer. The emission spectra were detected by a fiber-coupled CCD spectrometer (JY SPEX CCD3000).

Fig. 3 shows the emission spectra and the full-width half-maximum (FWHM) as a function of photon-pump energy for TPD, BMT-TPD and BMQ-TPD, which reflects their ASE characteristics. This spectral collapse is normally accompanied by a large enhancement of the output intensity and accounts for the presence of gain due to the stimulated emission. The specific parameters are listed in Table 1. These compounds show similar ASE characteristics, a significant increase of emission intensity and a rapid

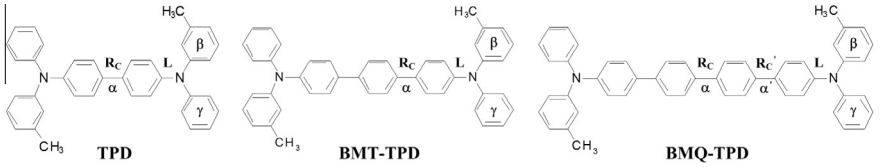

Fig. 1. Chemical structure of TPD, BMT-TPD and BMQ-TPD.

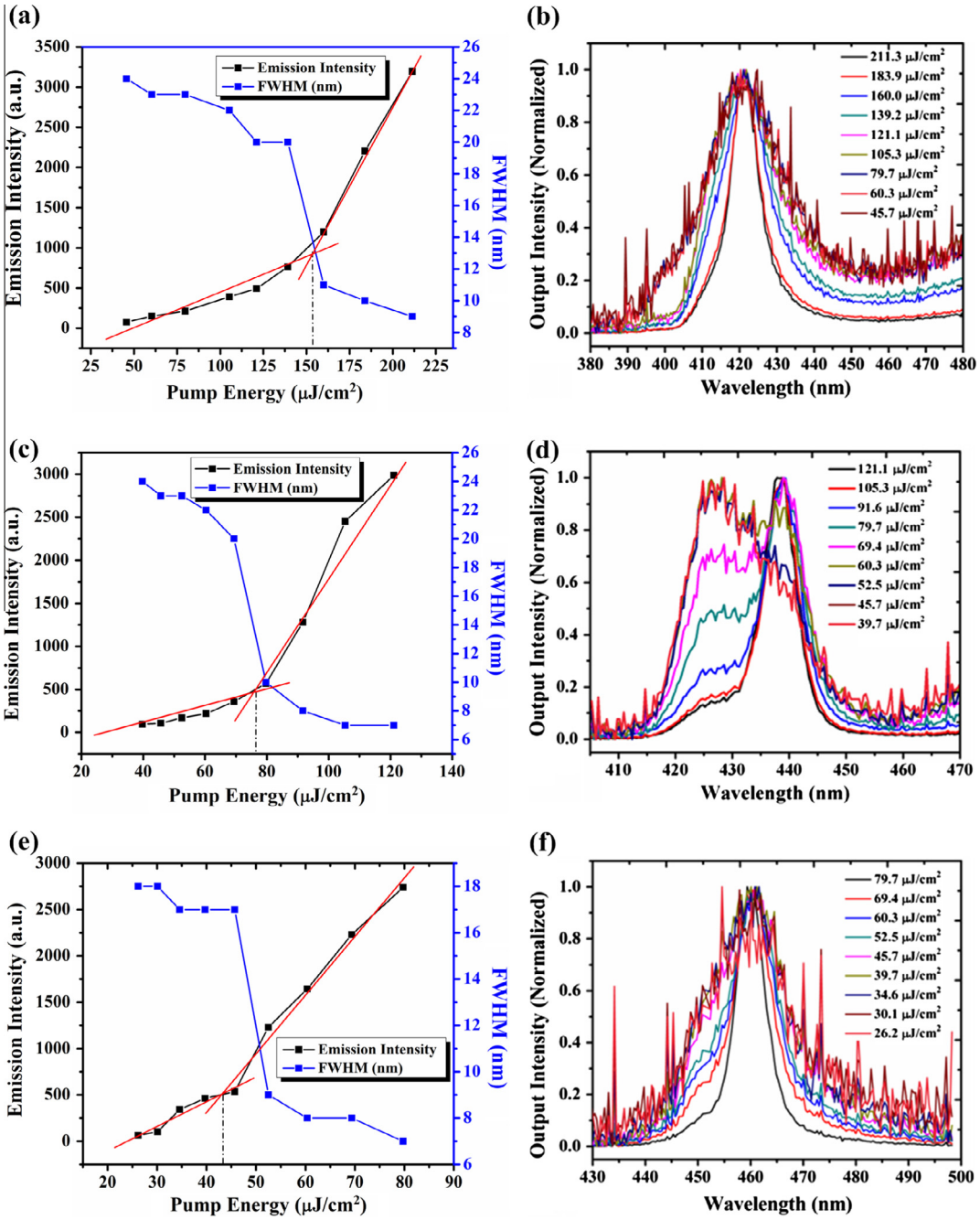

Fig. 3. The edge-emission spectra of TPD (a), BMT-TPD (c) and BMQ-TPD (e) excited by different energy. Output intensity at λ_{ASE} and Full Widths at Half-maximum (FWHM) as a function of pump energy for TPD (b), BMT-TPD (d) and BMQ-TPD (f).

decreasing of FWHM wavelength with an increased excitation intensity were observed. For all three compounds, the peaks of the narrowed emission take place at $\lambda = 421.4$ nm for TPD, $\lambda = 437.9$ nm for BMT-TPD and $\lambda = 459.4$ nm for BMQ-TPD respectively, which is consistent with vibration transition (0–1 transition) in PL spectra that is discussed in Section 2.1. The existence of shoulder peak is advantageous for population inversion compared with the other transitions. For three organic compounds, as observed in Fig. 3, the output intensity has a drastic increasing and the FWHM decreases to 9 nm, 7 nm and 7 nm when the pump energy reached to 153.7 μJ/cm^2, 77.1 μJ/cm^2 and 42.3 μJ/cm^2 respectively. Also, the ASE thresholds reduce with the increased number of central phenyl rings.

Resonant Raman Spectra were performed on a LabRam HR800 spectrometer (from Horiba Jobin Yvon) and measured using a 2400 groove/mm grating and the 325 nm (3.81 eV) emission line of a He–Cd laser. A ×15 nuv objec-

Table 1
Optical and ASE characteristics of three organic thin films.

Compound	TPD	BMT-TPD	BMQ-TPD
λ_{ASE}[a] (nm)	421.4	437.9	459.4
E_{th}[b] (μJ/cm^2)	153.7	77.1	42.3
FWHM[c] (nm)	9	7	7

[a] ASE peak wavelength.
[b] Excitation power threshold for ASE.
[c] Full width at half maximum of ASE spectrum.

tive lens was used to focus the laser to a diameter of 1 μm on the organic film surface. Each spectrum was obtained at room temperature recorded over a longer detection time of 120 s each testing from 200 cm^{-1} to 2000 cm^{-1}. All experiments were carried out at room temperature. The discussion of these results will be demonstrated in Section 3.3.

2.2. Geometry optimization with density functional theory

The ground-state and excited-state equilibrium molecular geometries of TPD, BMT-TPD and BMQ-TPD were optimized with DFT and TD-DFT using the hybrid functional B3LYP and the basis set 6-31g(d, p) respectively in the Gaussian 09 program package. Using the same functional and basis set, the vertical excitation energy was obtained with TD-DFT in the adiabatic approximation. The Stokes shift was obtained from the optimization of the geometry in the excited-state, and a projection of the deformation in the relaxed excited-state onto the vibrational eigenvectors defined the Huang–Rhys factor S_j for each vibrational mode $^{\hbar}\omega_j$ [15].

2.3. Elongation of vibrational modes

Under the adiabatic approximation, the electronic ground- and excited-state wave functions can be expressed as products of an electronic and nuclear part. Assuming a single vibronic coordinate for simplicity, the vibronic part of the total wave function contributes only a Frank-Condon overlap factors. Restricting the discussion to the lowest vibronic level $|0_e\rangle$ of the first excited-state vibronic as the initial state, the probability to emit through a transition to the electronic ground state vibronic level $|n_g\rangle$ with an electric field E at energy E_L is given by Fermi's golden rule [16]:

$$P(|0_e\rangle \rightarrow |n_g\rangle) = \frac{2\pi}{\hbar}\left|\vec{E}\cdot\vec{\mu}\right|^2 \left|\langle 0_e|n_g\rangle\right|^2 \times \delta(E_L + E_{HOMO} - E_{LUMO} - n_g{}^{\hbar}\omega) \quad (1.1)$$

where μ is the electronic transition dipole. The Franck–Condon factor can be expressed by a Poisson distribution:

$$\left|\langle 0_e|n_g\rangle\right|^2 = \frac{S^n}{n!}e^{-s} \quad (1.2)$$

In the Poisson distribution over the vibronic levels, S is Huang–Rhys factor which represents the vibronic coupling strength:

$$S_j = \frac{\omega(\Delta Q_j)^2}{2^{\hbar}} \quad (1.3)$$

where ΔQ_j represents the displacement along the normal mode $(NM)_j$ between the equilibrium positions of the two electronic states.

For the sake of the measured Raman-active modes corresponding to calculated internal vibrations, we determined their contributions to the reorganization energies. The reorganization energy $\lambda_j^{(g)}$ on the potential energy surface (PES) of the electronic ground state is expressed in terms of the Huang–Rhys factor S_j of the mode:

$$\lambda_j^{(g)} = S_j{}^{\hbar}\omega_j \quad (1.4)$$

The Stokes-Raman cross section for each mode $^{\hbar}\omega_j$ measured with an exciting laser energy of E_L can be expressed as [17]:

$$\sigma_R(\omega_j) \propto S_j\left[1 + \langle n(^{\hbar}\omega_j)\rangle\right] \times \left|A_0(E_L) - A_0(E_L - {}^{\hbar}\omega_j)\right|^2 \quad (1.5)$$

where $\langle n(^{\hbar}\omega_j)\rangle$ is the thermal occupation of the mode, S_j is normalized reorganization energy, and $A_0(E)$ the Kramers–Kronig transform of the optical absorption spectrum. As usual for the interpretation of resonant Raman spectra, we use only the leading term of the Taylor expansion [18]:

$$\sigma_R(\omega_j) \propto S_j\left[1 + \langle n(^{\hbar}\omega_j)\rangle\right](^{\hbar}\omega_j)^2 \quad (1.6)$$

3. Results and discussion

3.1. Optimized geometries and theoretical electronic transitions

To provide insight into the molecular geometries of all three compounds, we performed geometry optimizations within the framework of the density functional theory (DFT), using B3LYP/6-31G level. The notation for the dihedral angles and bond length in the molecular structures of TPD, BMT-TPD and BMQ-TPD are displayed in Fig. 1. TPD composes of a central biphenyl core and two twisted diphenylamine terminal wings, extended with methyl groups. In analog with TPD, BMT-TPD and BMQ-TPD have a central terphenyl core and central quaterphenyl core respectively.

The main geometric parameters of the three compounds are reported in Table 2. The value of the central torsion angle of crystal TPD compound, which is −34.7 (5) ° [19], is in good agreement with our calculation (Table 2). From the optimized geometry data, we obtained the twisted geometry in the ground state for the three compounds. However, the central dihedral angles become planar when going from S_0 to S_1, with a sharply varying from ∼35° to ∼10°, as shown by the large change in the central dihedral angle. Meanwhile, the central C—C single bond length is significantly shortened and the change of C=C double bond length can be barely observed (see Table 2). These features reveal that the difference in the molecular geometries (potential energy surfaces) for the two electronic states should play an important role in the dynamical process.

Based on the previous optimized ground state molecular geometries, theoretical calculations for all three

Table 2
Optimized geometries parameters of TPD, BMT-TPD and BMQ-TPD.

	TPD		BMT-TPD			BMQ-TPD	
	Ground[a]	Excited[b]	Ground[a]	Excited[b]		Ground[a]	Excited[b]
R_C	1.482 Å	1.440 Å	1.481 Å	1.448 Å	R_C	1.482 Å	1.446 Å
L	1.419 Å	1.430 Å	1.418 Å	1.426 Å	R_C'	1.481 Å	1.454 Å
α	35.0°	10.9°	−35.5°	−15.2°	L	1.417 Å	1.423 Å
β	40.1°	53.4°	39.7°	49.2°	α	−34.2°	−14.6°
γ	40.0°	53.5°	39.7°	49.2°	α'	36.5°	20.0°
					β	−36.9°	−45.8°
					γ	−37.0°	−45.8°

[a] Electronic ground state.
[b] The first excited states.

compounds predict the appearance of a very strong electronic transition (Table 3). The vertical transition is defined by a one-electron excitation from the highest occupied molecular orbital (HOMO) to the lowest unoccupied molecular orbital (LUMO), which were calculated at the B3LYP/6-31g(d, p) level using the TDDFT approach for TPD, BMT-TPD and BMQ-TPD. For all compounds, the dominant absorption band theoretically recorded at 364 nm, 376 nm and 382 nm are assigned to the HOMO to LUMO transition, being predicted at 354 nm, 358 nm and 364 nm in experiment separately.

Molecular structures influence the Frontier Molecular Orbital (FMO), we found that they possess similar spatial distribution. Comparing the FMOs in the ground state and the excited state, the three compounds exhibit some variations: HOMO in both geometries are rather localized over all phenyl rings and the CC bonds are π-bonding, whereas LUMO are mainly localized on the central phenyl and the CC bonds are π-antibonding, which spreads less over the peripheral phenyl groups in both geometries, as shown in Fig. 4. As the LUMO and HOMO are both mainly localized in the central phenyl rings, the geometric change in central phenyl mainly influence on the photophysics rather than diphenylamine terminal wings.

3.2. Vibrational frequencies and model PL spectra

On the basis of the optimized molecular geometries, the Huang–Rhys factors and reorganization energies of vibrational modes can be calculated by Franck–Condon approximation based on the vibrational frequencies according to the Eqs. ((1.1)–(1.4)). The electron-vibration constants S is proportional to the square of NM displacements. Hence, it can be concluded that the strength of electron-vibration is related to the deformation patterns ΔQ. Table 4 shows the specific data for some relevant vibrational modes.

The inner reorganization energies λ play a crucial role in the interpretation of the Stokes shift [13,14]. The total reorganization energies of the three compounds are 0.566 eV, 0.714 eV and 0.861 eV respectively (Table 4). According to absorption and PL spectra, the experimental Stokes shift are 0.419 eV, 0.503 eV and 0.577 eV, the values of 0.510 eV, 0.528 eV and 0.544 eV obtained from TD-DFT show a reasonable agreement. For TPD, BMT-TPD and BMQ-TPD, the enlarged total reorganization energy with the increased number of central phenyl rings leads to larger deformation patterns ΔQ and Huang–Rhys factors S. Hence, reinforced strength of electron-vibration were obtained, namely enhanced elongation of vibration modes.

A population inversion can be produced for the minimum vibronic level of the first electronic state relative to the non-equilibrium Franck–Condon levels of the ground state. To operative a four-level molecular band laser efficiently, the key factor is a major displacement from the ground state potential surface minimum to the excited state potential surface minimum. A change of molecular geometric conformation from the ground state to the first excited state would enable a four-level molecular band scheme to be operative. Moreover, the larger Stokes shift (reorganization energy) of BMT-TPD and BMQ-TPD relative to TPD indicate the large change of molecular geometry, which avails of four-level molecular band.

According to the analysis of vertical transition energy and the relevant parameters of vibrational modes, the PL spectra can be simulated. The various discrete vibronic transitions were calculated using vibrational progressions, which are related to Huang–Rhys factors S_j [18,20,21]. In the fitting procedure, FWHM were optimized in order to minimize the sum of the squares of the deviations between experimental and computed spectra. It was shown that the fitting was with a suitable Lorentzian broadening of FWHM = 0.093 eV which was adjusted manually to match

Table 3
TD-DFT//B3LYP/6-31G(d, p) vertical one-electron excitations related to the main peak in UV–Vis absorptions spectra of TPD, BMT-TPD and BMQ-TPD.

Compound	Experimental (nm)	TD-DFT//B3LYP/6-31G(d, p) (nm)	Oscillator strength, f	Description
TPD	354	364	1.0372	HOMO → LUMO
BMT-TPD	358	376	1.3891	HOMO → LUMO
BMQ-TPD	364	382	1.6082	HOMO → LUMO

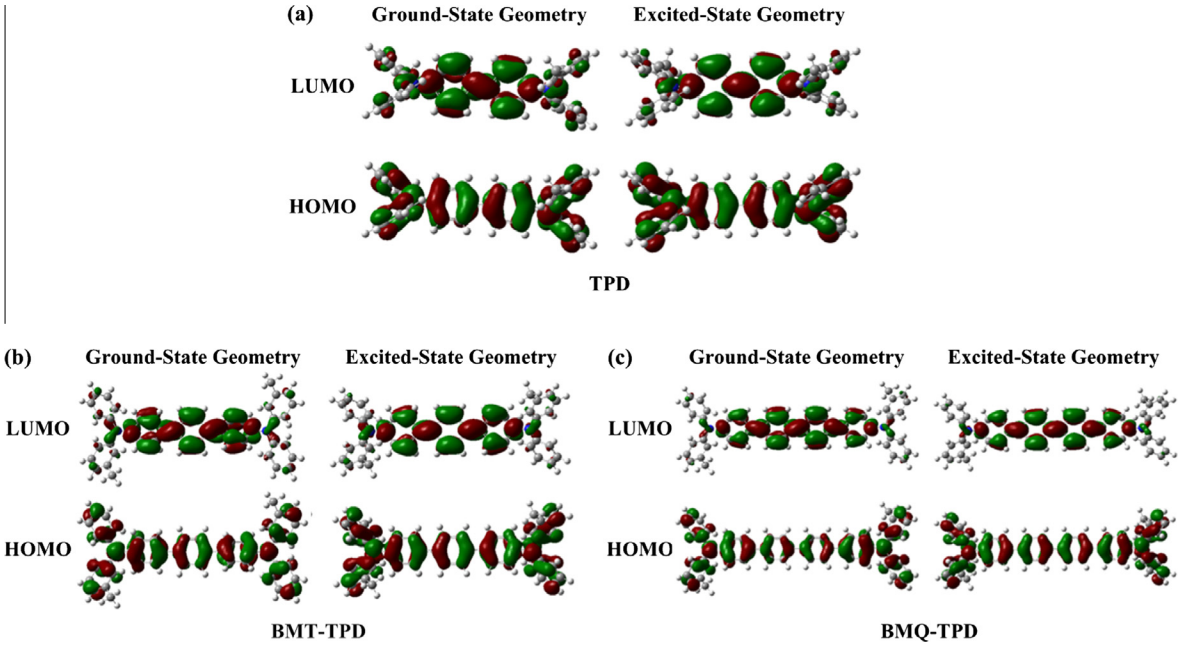

Fig. 4. Frontier molecular orbital in the ground-state and first exited-state geometry of TPD (a), BMT-TPD (b) and BMQ-TPD (c).

Table 4
The relevant parameters of the main strongly elongated internal modes.

TD-DFT//B3LYP								
TPD			BMT-TPD			BMQ-TPD		
$^{h}\omega_j$[a] (cm^{-1})	S_j[b] (1)	λ_j[c] (cm^{-1})	$^{h}\omega_j$[a] (cm^{-1})	S_j[b] (1)	λ_j[c] (cm^{-1})	$^{h}\omega_j$[a] (cm^{-1})	S_j[b] (1)	λ_j[c] (cm^{-1})
						7	0.59	4.4
						8	35.095	386.5
23	0.202	4.7	7	89.004	664.2	11	0.598	15.1
31	1.76	54.1	13	0.103	1.3	13	0.976	28.3
36	3.333	118.8	24	0.415	9.8	15	0.737	28.7
43	0.335	14.2	33	0.07	9.5	53	0.366	19.7
49	5.498	271.9	45	0.213	2.3	54	0.407	22.1
66	1.072	70.9	46	0.119	5.4	60	0.827	49.7
87	0.155	13.6	49	0.06	2.9	74	2.0165	159.8
95	3.564	340.2	83	2.048	169.6	91	0.884	80.5
426	0.119	50.6	422	0.078	32.8	97	4.0983	483.2
780	0.072	56.2	429	0.081	34.8	104	0.113	11.8
						118	0.806	94.9
			1222	0.114	139.6	1226	0.133	162.5
1215	0.109	82.6	1319	0.052	55.6	1318	0.07	91.4
1309	0.051	66.4	1650	0.057	94.9	1650	0.053	87.4
1654	0.07	115.3	1653	0.08	132	1653	0.102	167.8
1664	0.151	251.6	1662	0.121	201.2	1660	0.137	227.5

[a] Vibrational frequencies.
[b] Huang–Rhys factors.
[c] Reorganization energies.

the corresponding experiment spectra. Based on the discussion about theoretical electronic transitions in Section 3.1, the lowest transition energy for the excited-state geometry calculated at the B3LYP/6-31g(d, p) level is 2.89 eV, 2.76 eV and 2.69 eV, which is only about 0.19 eV, 0.20 eV and 0.15 eV below the maximum of the measured PL. The calculated PL spectra are in excellent agreement with the experimental PL spectrum, for the main peak (402 nm, 420 nm and 438 nm) and first subband (421 nm, 442 nm and 458 nm).

Fig. 5 shows that the different discrete energy levels cluster together, which merge into a large band and two apparent sidebands. For BMT-TPD and BMQ-TPD, more centralized and stronger intensity discrete energy levels were obtained compared with TPD. It can be concluded that the vibronic band intensity reinforced with the

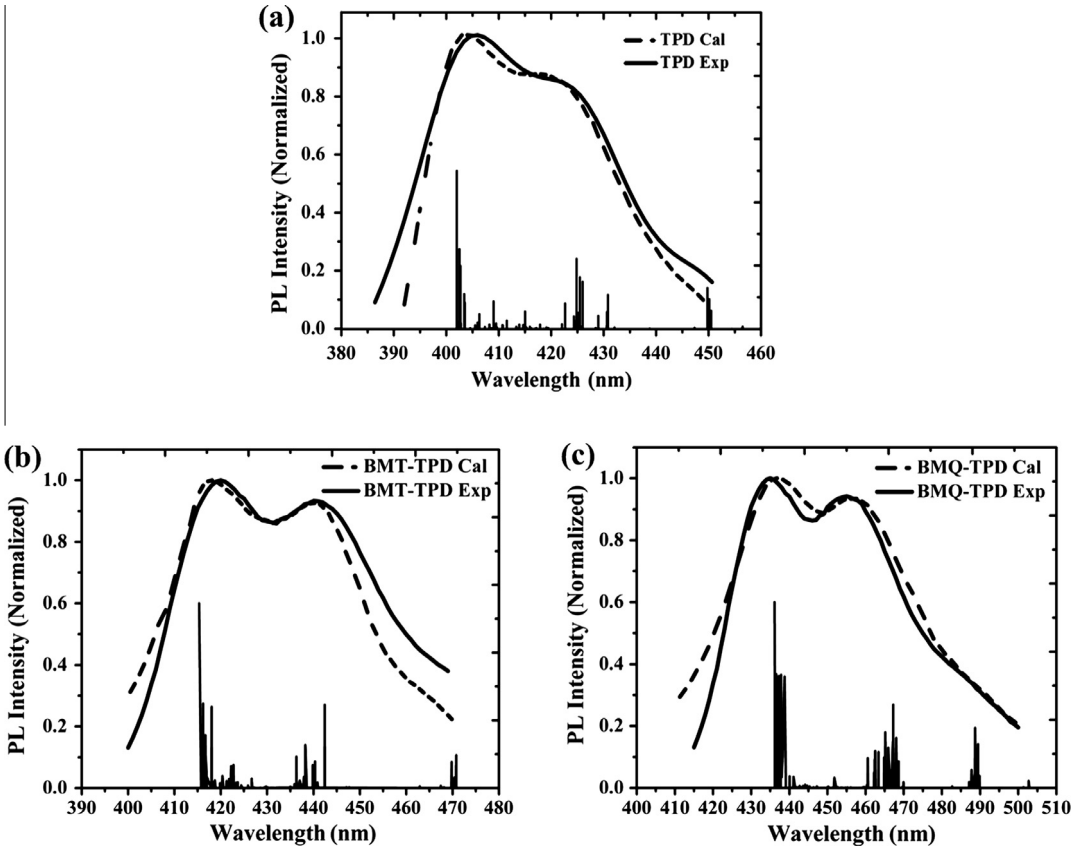

Fig. 5. Model simulation (dashed lines) of the linear PL of TPD, BMT-TPD and BMQ-TPD compounds according to Table 4. Discrete vertical bars, normalized to the height of the main peak, is discrete vibronic transitions.

increased number of central phenyl rings deriving from enhanced elongation of high-frequency modes, which result in a relative weak broadening in PL spectra line width. In the modelling PL spectra of BMT-TPD and BMQ-TPD, a small number of discrete energy levels exist between the main peak and the vibronic subbands. Beyond that, the centralized discrete energy levels would bring out more legible energy level distribution. Generally, higher intensity vibronic peak and more clear energy level scheme is favorable for the formation of four-level molecular band scheme for population inversion.

3.3. Resonant Raman spectra and vibrational modes

We measured the Raman spectra of the blends of TPD, BMT-TPD and BMQ-TPD within PS. The blend film was spin-coated on glass substrates. As shown in Fig. 6, we found that the dominant vibrational modes in the Raman spectra of all three compounds own the same frequencies, corresponding to their uniform high-frequency modes within the central carbon rings. The spectra are dominated by several distinct peaks between 400 cm^{-1} and 1700 cm^{-1}, with few features below 400 cm^{-1} and around 3000 cm^{-1} (not shown). In the range of 1000–1700 cm^{-1}, the vibrations mainly arise from the elongation in the plane of the various phenyl rings.

In low-frequency internal vibrations modes (0–1000 cm^{-1}), the Raman intensity of three compounds are weak (Fig. 6). As shown in Table 4, below 1000 cm^{-1}, the small number of the major low-frequency modes of TPD, BMT-TPD and BMQ-TPD are 10, 10 and 13 respectively, and all the modes are torsional modes [22]. They all have out-of-plane C—C torsional mode within the whole molecule and torsional modes arising form central phenyl core or terminal wings. The small number and weak elongation of low-frequency modes result in less energy level existing between the main peak (0–0 transition) and the vibronic (0–1 transition) peak [15], which coincide with Fig. 5.

For all compounds, the strongly elongated high-frequency modes contribute to the first vibronic peak (0–1 transition) in the PL spectra, which form an effective "four-level" system for lasing. In high-frequency modes (1000–1700 cm^{-1}), the intensity patterns are different in Raman spectra, and the high-frequency modes frequencies at around 1200 cm^{-1}, 1300 cm^{-1}, 1650 cm^{-1} (Fig. 6 and Table 4) in the three compounds owes to the C—H in plane bend, C—C inter-ring stretching and C—C intra-ring stretching modes in the central phenyl rings as shown in Fig. 7. It is remarkable to observe that the high-frequency ($\geqslant$1000 cm^{-1}) vibrational peak intensity in the resonant Raman spectra strengthens with the increased number of central phenyl rings. Especially, for the high-frequency

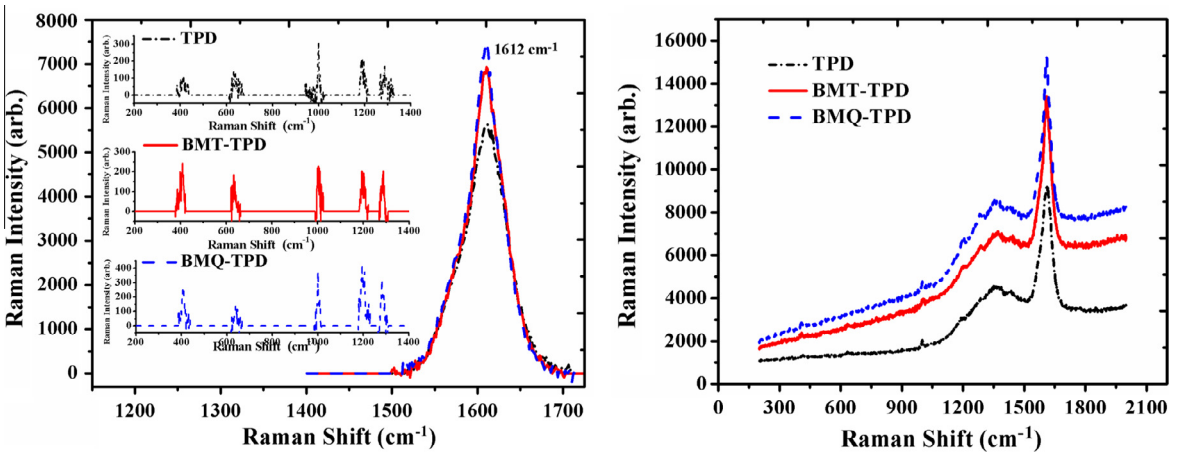

Fig. 6. Resonant Raman Spectra of TPD, BMT-TPD and BMQ-TPD diluted in toluene solution containing PS deposited on glass substrates, obtained with the 325 nm emission line.

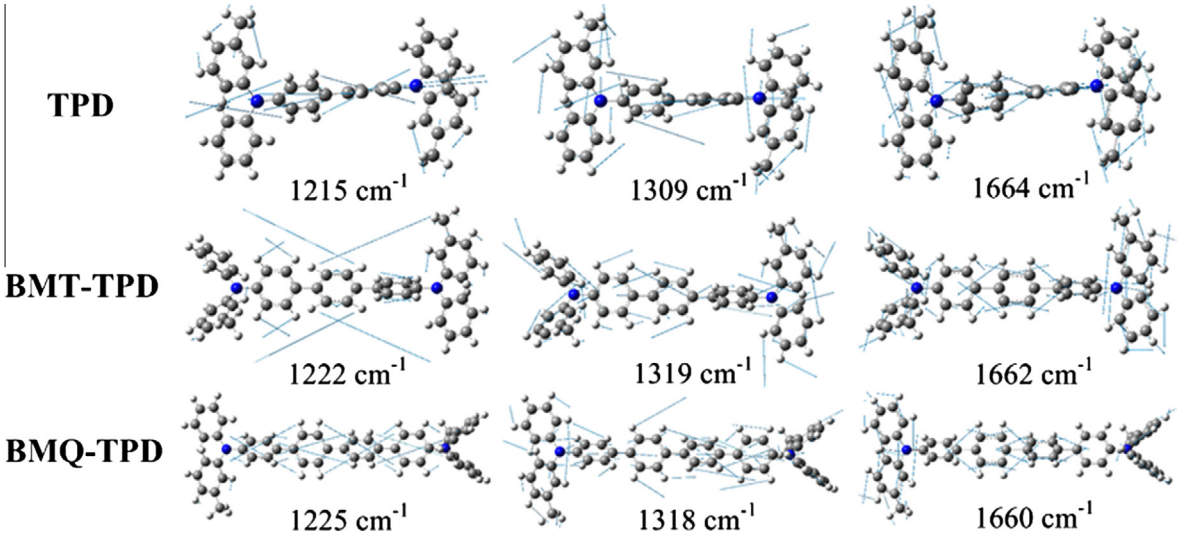

Fig. 7. Calculated vibrational eigenvectors of dominating vibrational modes: the similar high-frequency modes for TPD, BMT-TPD and BMQ-TPD. The contribution of each mode to the total deformation of samples is enlarged by a same factor.

mode at 1612 cm^{-1}, it corresponds to vibrational energy level splitting of 0.2 eV. BMQ-TPD possesses the maximum Raman intensity, followed by BMT-TPD and TPD. The higher Raman intensity means an enhanced elongation high-frequency mode. Hence, the strong vibrational modes correspond to high intensity vibronic peak, which participate in establishing vibrational energy level of the four-level scheme.

Generally speaking, the enhanced elongation internal vibrations of high-frequency modes derive from the increased number of central phenyl rings [23]. The elongation of high-frequency modes contribute to the higher first vibronic peak in PL spectra and the elongation of low-frequency modes results in a broadening of the vibronic subbands defined by the high-frequency modes [13–16]. Relative small number of low-frequency modes would bring out a distinct energy level system between two energy levels which root in the main peak and the shoulder peak. Enhanced elongation of high-frequency vibrational modes dedicate to the vibrational energy level contained within four-level energy level schemes.

3.4. Four-level energy level scheme

The discrete vibronic transitions in PL spectrum exhibited different energy levels in the ground state (Fig. 8). Fig. 8 shows the energy levels of both the ground and the first excited singlet states. In each state, the electronic level is divided into vibronic sublevels. The spacing of these sublevels is approximately 0.15 eV, and thus there is little thermal excitation from the lowest level at room temperature. In the four-level molecular band scheme, levels I and III are the zero-point vibronic levels corresponding to the singlet electronic ground state S_0 and the first excited state

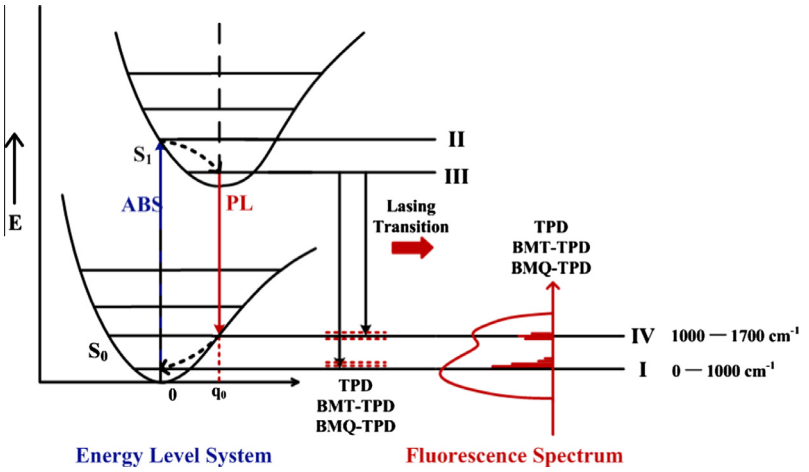

Fig. 8. Four-level system of TPD, BMT-TPD and BMQ-TPD reflected from the relation between the optical spectra and vibronic levels.

S_1 [24]. The vibronic levels II and IV represent the (thermally) non-equilibrium vibronic levels of the states S_0 and S_1, respectively. The levels II and IV may lie within some Franck–Condon vibronic levels for the corresponding absorption, fluorescence and may represent partially resolved vibronic bands. The vibronic levels II and IV are excited as probable Franck–Condon transitions and are rapidly equilibrated by intramolecular vibrational relaxation. These four vibronic levels compose the four-level system and the population inversion take place between level III and IV.

For the three compounds, in accordance with our previous work [15], a small number of low-frequency modes corresponding to distinct sideband result in uncontinuous energy levels between level I and IV, II and III. The vibrational splitting from the main peak and the first vibronic subband, resulting from strongly elongated high-frequency modes, is 0.14 eV, 0.13 eV and 0.13 eV, respectively. When samples were photopumped, pump laser can excite the molecule from the zero-point vibronic level in the ground state (I) to an excited vibrational level (II) vertically in the first excited singlet state, which will be followed by rapid thermal relaxation to the zero-point vibronic level (III) of the excited singlet state. Due to the "four-level" system mechanism, lasing can take place via the transition from the lowest excited singlet state to the first vibronic sublevel of ground state, which is followed by rapid relaxation to the bottom of ground state. The thermal relaxation rate within the vibronic manifold is faster than the emission process [25]. For BMT-TPD and BMQ-TPD, along with the increased number of central phenyl rings, the enhanced elongation of high-frequency modes relative to TPD bring out distinct energy-level configuration, which is more favorable to constitute vibronic level I, II, III and IV. Hence, the energy levels scheme of these organic semiconductors enable to achieve effective population inversion between III and IV. A large amount of population inversion realized even when most compounds are in the ground state, so lasing can be obtained for a very low rate of excitation, which is the low threshold for lasing. The "four-level" system also explains why the emission occurs at longer wavelength than the absorption.

4. Conclusion

In conclusion, we developed two deep-blue lasing materials: BMT-TPD and BMQ-TPD, which exhibited enhanced ASE characteristics at the first subband of PL spectra and lower threshold compared with TPD. In theory, the less elongated low-frequency modes produce an appreciable energy gap between the bottom and the first vibronic sublevel of ground state. Moreover, we have shown that, accompanying with the increased number of central phenyl rings, the enhanced elongation of C—H bending and C—C stretching high-frequency modes in central carbon ring contribute to the more distinct vibronic sublevels of ground state observed in PL spectra (the subbands). More distinct energy level scheme is conductive to form an effective "four-level" system for population inversion, which brings out the significant lower thresholds.

Acknowledgements

This work was financially supported by Basic Research Program of China (2013CB328705), National Natural Science Foundation of China (Grant Nos. 61275034, 61106123), Ph.D. Programs Foundation of Ministry of Education of China (Grant No. 20130201110065); Fundamental Research Funds for the Central Universities (Grant No. xjj2012087).

References

[1] W. Zapka, U. Brackmann, Shorter dye laser wavelengths from substituted p-terphenyls, Appl. Phys. 20 (1979) 283–286.
[2] H.R. Haghighi, S. Forget, S. Chénais, A. Siove, M. Castex, Laser operation in nondoped thin films made of a small-molecule organic red-emitter, Appl. Phys. Lett. 95 (2009) 033305.
[3] S.Y. Ma, T. Nakajima, K. Yamashita, Solid state organic laser emission at 970 nm from dye-doped fluorinated-polyimide planar waveguides, Appl. Phys. Lett. 93 (2008) 023306.

[4] G. Tsiminis, Y. Wang, P.E. Shaw, A.L. Kanibolotsky, I.F. Perepichka, M.D. Dawson, P.J. Skabara, G.A. Turnbull, Low-threshold organic laser based on an oligofluorene truxene with low optical losses, Appl. Phys. Lett. 94 (2009) 243304.
[5] N. Tada, S. Tatsuhara, A. Fujii, Y. Ohmori, K. Yoshino, Nonlinear emission from 8-hydroxyquinoline aluminum and diamine derivative superlattice structures excited by third-harmonic-generation from Nd:YAG laser light, Jpn. J. Appl. Phys. 36 (1997) L421–L424.
[6] S. Pfeiffer, H.-H. Hörhold, H. Boerner, N. Nikol, W. Busselt, Vinylene-bridged triphenylamine dimers as an emitting material in trilayer organic electroluminescent devices, SPIE 3476 (1998) 258–266.
[7] W. Holzer, A. Penzkofer, H.-H. Hörhold, Travelling-wave lasing of TPD solutions and neat films, Synth. Met. 113 (2000) 281–287.
[8] M.A. Díaz-García, S.F. de Ávila, M.G. Kuzyk, Dye-doped polymers for blue organic diode lasers, Appl. Phys. Lett. 80 (2002) 4486–4488.
[9] M.A. Díaz-García, E.M. Calzado, J.M. Villavilla, P.G. Boj, J.A. Quintana, M. Kuzyk, TPD-based blue organic lasers, J. Nonlin. Opt. Phys. Mater. 13 (2004) 621–626.
[10] E.M. Calzado, J.M. Villavilla, P.G. Boj, J.A. Quintana, M.A. Díaz-García, Concentration dependence of amplified spontaneous emission in organic-based waveguides, Org. Electron. 7 (2006) 319.
[11] D. Schneider, T. Rabe, T. Riedl, T. Dobbertin, O. Werner, Deep blue widely tunable organic solid-state laser based on a spirobifluorene derivative, Appl. Phys. Lett. 84 (2004) 4693–4695.
[12] Y. Kawamura, H. Yamamoto, K. Goushi, H. Sasabe, C. Adachi, Ultraviolet amplified spontaneous emission from thin films of 4,4′-bis(9-carbazolyl)-2,2′-biphenyl and the derivatives, Appl. Phys. Lett. 84 (2004) 2724–2726.
[13] I. Vragovic, E.M. Calzado, M.A. Díaz-García, The structure and energetics of TPD ground and excited states, Chem. Phys. 332 (2007) 48–54.
[14] R. Scholz, L. Gisslén, C. Himcinschi, I. Vragovic, E.M. Calzado, E. Louis, E. San Fabian, M.A. Díaz-García, Asymmetry between absorption and photoluminescence line shapes of TPD: spectroscopic fingerprint of the twisted biphenyl core, J. Phys. Chem. A 113 (2009) 315–324.
[15] Z. Wu, L. Ma, P. Liu, C. Zhou, S. Ning, A. El-Shafei, X. Zhao, X. Hou, Structure–property relationship of amplified spontaneous emission in organic semiconductor materials: TPD, DPABP, and NPB, J. Phys. Chem. A 117 (2013) 10903–10911.
[16] I. Vragovic, R. Scholz, M. Schreiber, Model calculation of the optical properties of 3,4,9,10-perylene-tetracarboxylic-dianhydride (PTCDA) thin films, Euro. Phys. Lett. 57 (2002) 288–294.
[17] N.E. Gruhn, D.A. da Silva Filho, T.G. Bill, M. Malagoli, V. Coropceanu, A. Kahn, J.-L. Brédas, The vibrational reorganization energy in pentacene: molecular influences on charge transport, J. Am. Chem. Soc. 124 (2002) 7918–7919.
[18] R. Scholz, A.Y. Kobitski, T.U. Kampen, M. Schreiber, D.R.T. Zahn, Resonant Raman spectroscopy of 3,4,9,10-perylene-tetracarboxylic-dianhydride epitaxial films, Phys. Rev. B 61 (2000) 13659–13669.
[19] A.R. Kennedy, W.E. Smith, D.R. Tackley, W.I.F. David, K. Shankland, K. Brown, Tetraaryl biphenyl diamine hole transport materials: a structural study utilizing both single crystal and high resolution powder diffraction, J. Mater. Chem. 12 (2002) 168–172.
[20] E. Peeters, A.M. Ramos, S.C.J. Meskers, R.A.J. Janssen, Singlet and triplet excitations of chiral dialkoxy-p-phenylene vinylene oligomers, J. Chem. Phys. 112 (2000) 9445–9454.
[21] Q. Peng, Y. Yi, Z. Shuai, J. Shao, Toward quantitative prediction of molecular fluorescence quantum efficiency: role of Duschinsky rotation, J. Am. Chem. Soc. 129 (2007) 9333–9339.
[22] R. Scholz, M. Schreiber, Linear optical properties of perylene-based chromophores, Chem. Phys. 325 (2006) 9–21.
[23] G. Heimel, M. Daghofer, J. Gierschner, E.J.W. List, A.C. Grimsdale, K. Müllen, D. Beljonne, J. Brédas, E. Zojer, J. Chem. Phys. 122 (2005) 054501.
[24] J. Carlos del Valle, M. Kasha, J. Catalán, Spectroscopy of Amplified Spontaneous Emission Laser Spikes in Phenyloxazoles. Prototype Classes, J. Phys. Chem. A 101 (1997) 3260–3272.
[25] V. Bernard, Characteristics of fluorescence emission, Molecular Fluorescence: Principles and Applications, Wiley-VCH Verlag, New York, 2001, p. 35 (Chapter 3).